SCIENTIFIC REPORTS

OPEN

SUBJECT AREAS:
CALCIUM SIGNALLING
SODIUM CHANNELS

Received
28 August 2013

Accepted
22 April 2014

Published
14 May 2014

Correspondence and requests for materials should be addressed to A.K.B. (amal@iitm.ac.in)

* Current address: Research Group Neuroplasticity, Leibniz Institute for Neurobiology, Magdeburg, Germany.

Pannexins form gap junctions with electrophysiological and pharmacological properties distinct from connexins

Giriraj Sahu*, Sunitha Sukumaran & Amal Kanti Bera

Department of Biotechnology, Indian Institute of Technology Madras, Sardar Patel Road, Chennai - 600036, Tamil Nadu, India.

Stable expression of pannexin 1 (Panx1) and pannexin 3 (Panx3) resulted in functional gap junctions (GJs) in HeLa cells, but not in Neuro-2a (N2a) or PC-12 cells. The glycosylation pattern of expressed Panx1 varied greatly among different cell lines. In contrast to connexin (Cx) containing GJs (Cx-GJs), junctional conductance (G_j) of pannexin GJs (Panx-GJs) is very less sensitive to junctional voltage. Both Panx1 and Panx3 junctions favoured anionic dyes over cations to permeate. Though, carbenoxolone (CBX) and probenecid blocked Panx1 hemichannel activity, they had no effect on Panx1-GJs or Panx3-GJs. Extracellular loop 1 (E1) of Panx1 possibly bears the binding pocket. The Cx-GJ blocker heptanol blocked neither Panx1 hemichannel nor Panx-GJs. Unlike the GJs formed by most Cxs, CO_2 did not uncouple Panx-GJs completely. Oxygen and glucose deprivation (OGD) caused lesser uncoupling of Panx-GJs compared to Cx43-GJs. These findings demonstrate properties of Panx-GJs that are distinctly different from Cx-GJs.

Pannexins are the recently discovered vertebrate proteins, homologous to the invertebrate gap junction (GJ) forming proteins, innexins[1]. In humans three pannexins, namely pannexin 1 (Panx1), pannexin 2 (Panx2) and pannexin 3 (Panx3), are known to be expressed[1,2]. Panx1 is expressed abundantly in brain and in many other organs such as bladder, testis, and ovary[1–3], whereas the expression of Panx2 is mostly limited to brain[2–5]. Panx3 is expressed in skin, cartilage, heart, kidney and cochlea[6–8]. Panx1 hemichannels have been implicated in ATP release, calcium signalling, keratinocyte and osteoblast differentiation, taste reception, cell death, post-ischemic neurodegeneration, tumour suppression and seizure[8–13]. Several mechanisms have been shown to open Panx1 hemichannels. For example, Panx1 hemichannels can be activated by depolarization, extracellular K^+ and mechanical stress[14–16]. Basally inactive human Panx1 gets activated by the caspase-cleavage of its carboxy terminus, which possibly occludes the channel pore from the intracellular side[17,18]. Panx1 associates with $P2X_7$ receptors to form a large pore[19–21]. $Panx1^{-/-}$ and $Panx2^{-/-}$ mice developed smaller infarcts in experimental stroke, suggesting their involvement in ischemic neuronal death[12].

Although the predicted topology of Panxs is very similar to that of connexins (Cxs), its ability to form cell-cell junctional channel is controversial. Bruzzone et al., 2003, first demonstrated the formation of Panx1-GJs in the *Xenopus* oocyte heterologous expression system[3]. Similarly, over-expression of Panx1 formed functional GJs in C6 glioma cell line that allowed the passage of sulforhodamine 101 dye[10]. Panx1 also appeared to form calcium permeable GJs in LNCaP human prostate cancer cell line[9]. Very recently, over-expressed Panx3 has been shown to form calcium permeable junctions in C2C12 cells[8]. On the contrary, several groups argued against the ability of Panxs to form GJs[6,22,23]. The existing reports favouring Panx-GJs have been suspected as an outcome of the up-regulation of endogenous connexins. The main reason for this scepticism lies in the characteristic of Panxs to be glycosylated at the extracellular loops. Unlike Cxs, Asn 254 of second extracellular loop (E2) of Panx1 is glycosylated, whereas first extracellular loop (E1) of Panx3 bears the glycosylation site[6,24]. It has been proposed that glycosylation at an extracellular loop renders Panx hemichannels incapable of docking with neighbouring hemichannels to form GJs. However, experimental evidence supporting Panx-GJs cannot be ignored completely.

In the present study, we clearly demonstrate the formation of Panx1-GJs and Panx3-GJs in a cell specific manner. Both Panx1 and Panx3 formed GJs in HeLa cells but not in N2a or PC-12 cells. Functional GJs, observed upon stable expression of Panx1 and Panx3 are not Cx-GJs formed from up-regulated endogenous Cxs. Here we

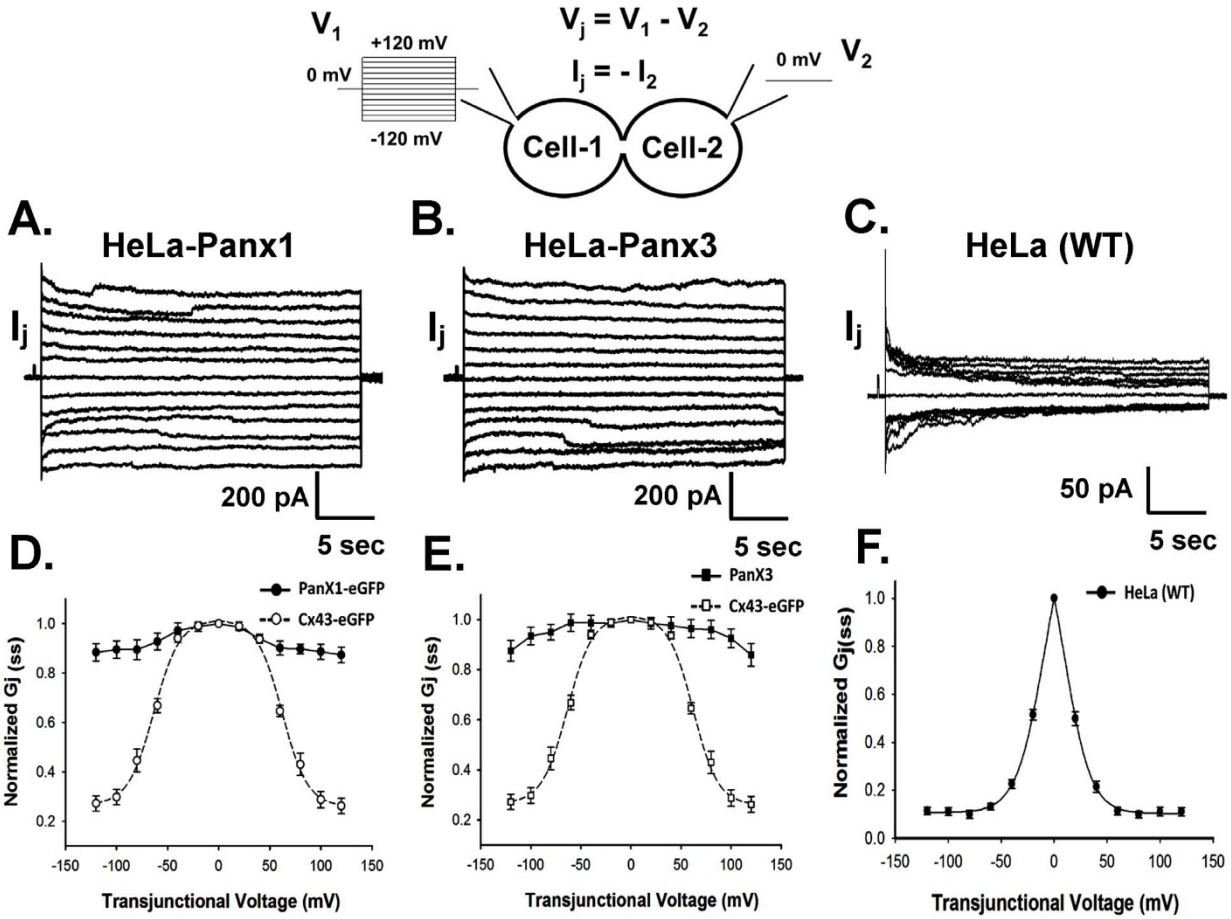

Figure 1 | Panx1 and Panx3 form functional gap junctions (GJs) in HeLa cell. The cartoon diagram represents recording of junctional currents using dual patch clamp. Series of voltage (V_1) steps were applied to cell-1, keeping the voltage of cell-2 (V_2) constant at 0 mV. Junctional current (I_j) corresponds to the current recorded from cell-2. Representative I_j traces are depicted in (A, B and C). Panx1 and Panx3 (A and B) transfected cells exhibited significant I_j. (C) non-transfected control HeLa cells showed much less I_j, compared to Panx1 and Panx3 expressing cells. (D and E) V_j-$G_{j(ss)}$ plots of Panx1 and Panx3 compared with that of Cx43. $G_{j(ss)}$ of both Panx1 and Panx3 remained relatively unchanged with increasing V_j. $G_{j(ss)}$ of Cx43 showed voltage dependence in similar experimental conditions. Values are the mean ± SEM of 4–11 independent experiments. The dashed line in the Cx43 plot represents the fitted curve with the two states Boltzmann equation. (F) V_j-$G_{j(ss)}$ plot of endogenous GJ, recorded from non-transfected wild type (WT) HeLa cells (n = 7). The sharp decrease of $G_{j(ss)}$ with increasing V_j resembles the V_j-G_j relation of Cx45-GJs.

report electrophysiological and pharmacological characteristics of Panx-GJs. Unlike Panx hemichannels, Panx-GJs are insensitive to CBX and probenecid. A possible mechanism of the inhibitor insensitivity of Panx1-GJs is discussed.

Results

Pannexins form functional gap junctions in cell specific manner. We generated stable HeLa and PC-12 cells, expressing Panx1-eGFP (from here on Panx1 means Panx1-eGFP) or Panx3. Both Panx1 and Panx3 were expressed transiently in N2a cells. Representative pictures of HeLa cells expressing Panx1 or Panx3 are shown in supplementary figure 1. Panx1 expression was confirmed by GFP fluorescence at the membrane surface. The expression of Panx3 was confirmed by immunofluorescence using an anti-Panx3 antibody. The membrane expression pattern of Panx3 was found similar to Panx1 (Supplementary Figure 1).

Electrophysiological properties of Panx-GJs were studied using dual voltage clamp and applying trans-junctional voltage (V_j) steps ranging from −120 mV to +120 mV to one of the cells of a coupled pair. Junctional currents (I_j) were measured from the second cell. HeLa-Panx1 and HeLa-Panx3 stable cells showed almost linear rise of I_j with increasing V_j (Figure 1A, 1B). Unlike most Cx-GJs, the V_j dependent inactivation of both Panx1- and Panx3 I_j were very less and can only be observed at very high V_j (≥80 mV), which is in accordance with an earlier report[3]. As shown in figure 1D and 1E, steady state junctional conductance ($G_{j(ss)}$) only changed a little with the change of V_j. Cx43-GJ in the same experimental conditions showed sharp decrease of $G_{j(ss)}$ with increasing V_j (Figure 1D, 1E). The average I_j recorded from Panx1 and Panx3 stable HeLa cells at 100 mV were 1090 ± 148 pA (n = 31) and 927 ± 90 pA (n = 27) respectively. Very weak coupling was observed in non-transfected control cells. Average instantaneous I_j was 57 ± 7 pA (n = 25) at 100 mV (Figure 1C). Steady state junctional currents ($I_{j(ss)}$), obtained from control HeLa cells showed enormous V_j sensitivity. As shown in figure 1F, $G_{j(ss)}$ of endogenous junctions reduced sharply with increasing V_j. $I_{j(ss)}$ recorded from Cx43 transfected cells and control cells were successfully fitted with two state Boltzmann equation, but not for Panx1 and Panx3 stable cells. Interestingly, neither Panx1 nor Panx3 formed functional GJs in stable transfected PC-12 cells and in transiently transfected N2a cells, though surface expression was observed (data not shown). This suggests that Panxs form functional GJs, but in a cell specific manner.

Greater glycosylation is associated with failure to form Panx-GJs. To determine if differential glycosylation is the reason behind cell specific formation of Panx-GJs, we compared Panx1-eGFP protein expressed in HeLa, N2a and PC-12 cells. As shown in figure 2A and

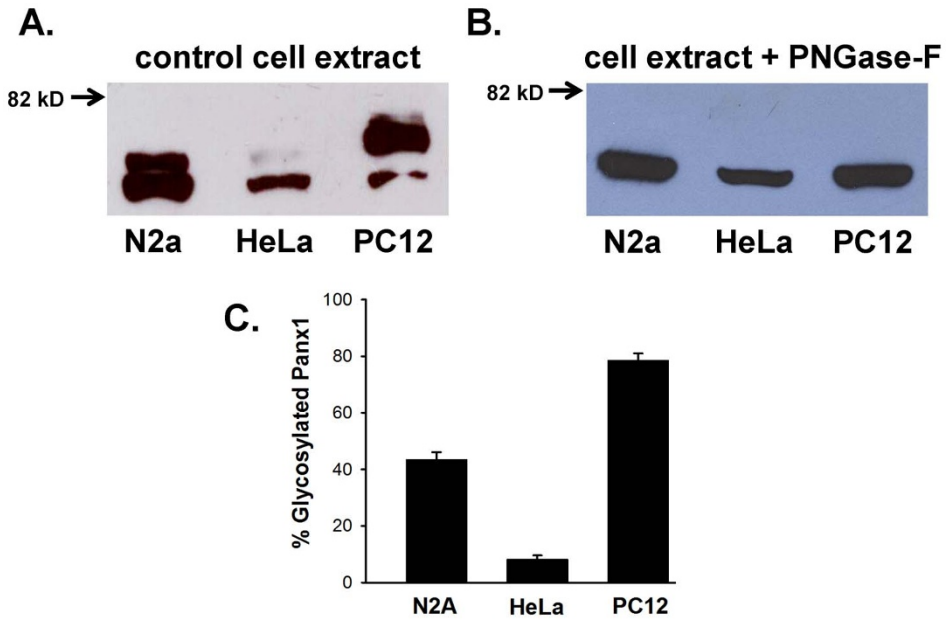

Figure 2 | Differential glycosylation pattern of Panx1. (A) Representative western blots of Panx1-eGFP, expressed in N2a, HeLa and PC-12 cells. 50 μg of total proteins were resolved on 7.5% SDS-polyacrylamide gel. The protein was transferred to PVD membrane and probed with anti-GFP antibody. The higher molecular weight band corresponds to the glycosylated form. (B) The glycosylated Panx1 band disappeared upon treatment with 10 units of PNGase-F for 30 minutes. Corresponding bands of Panx1 (A and B) are cropped from the full blots and presented. Picture of the full-length blots are shown in supplementary section. (C) Comparison of the glycosylated fraction of Panx1 in different cell lines. In N2a and PC-12 cells, 43 ± 3% and 79 ± 3% of total Panx1 are glycosylated, whereas, in HeLa cells, glycosylated fraction represents only 8 ± 2% of total Panx1. Band intensity was quantified with Image J software. Values are the mean ± SEM of seven experiments.

supplementary figure 5A, anti-GFP antibody recognized 2 prominent bands in all three cells used. The specificity of anti-GFP antibody was verified using cell lystaes prepared from control or eGFP-expressed cells. As shown in supplementary figure 5B, the antibody did not cross-react with any endogenous protein (negative control). Transfected cells (positive control) showed single GFP band.

According to a previous report[6], the upper band (Fig. 2A) corresponds to the glycosylated form of Panx1. To verify this, we treated the cell extracts with deglycosylase enzyme, PNGase-F. As shown in figure 2B and supplementary figure 5C, the upper band completely disappeared in PNGase-F treated samples, confirming their glycosylation status. Interestingly, the pattern of glycosylation varied significantly among different cell lines. Unlike in HeLa cells, Panx1 expressed in N2a and PC-12 cells is highly glycosylated. Data averaged from seven independent experiments revealed that 79 ± 3% and 43 ± 3% of total Panx1 are glycosylated in PC-12 and N2a cells compared to only 8 ± 2% in HeLa cells (Figure 2C). These observations suggest that glycosylation of Panx1 in PC-12 and N2a cells may hinder the formation of GJs. We could not perform similar experiments with Panx3 due the poor quality of commercially available antibodies for western blotting.

We treated the Panx1 and Panx3 expressing N2a and PC-12 cells with PNGase-F to see whether removal of glycan chain induces GJ formation. However, no junctional currents were detected after 2–3 hours, following PNGase-F treatment.

Endogenous connexins. To verify if I_j recorded from Panx1 and Panx3 expressing HeLa cells, were due to Panx1 and Panx3, and not from up regulated endogenous Cxs, we quantified mRNA levels of different Cxs and Panxs by real time PCR. Consistent with previous reports[25], endogenous Cx26, Cx31.1 and Cx45 mRNAs were detected in wild type HeLa cells (Table 1 and Supplementary Figure 2), though there is another report[26] showing absence of the Cx26 in HeLa cells. We could not detect Cx30, Cx37, Cx40, Cx43, Cx46 and Cx50 in wild type, Panx1 or Panx3 stable-transfected HeLa cells. To assure that the negative results did not arise from the inhibition of qPCR, we performed qPCR inhibition assay between cell samples. As shown in supplementary table 2, ΔC_T values for all the samples are less than 2, confirming no inhibition of qPCR. Cx31.1 does not form functional GJs[27]. The weak coupling observed in wild type HeLa cells is possibly due to the presence of very low level of Cx45-GJs as the V_j-$G_{j(ss)}$ plot showed a sharp decrease of $G_{j(ss)}$ with increasing V_j (Figure 1F), a typical characteristic of Cx45 junction[28]. Stable expression of Panx1 and Panx3 did not increase Cx45 mRNA significantly (Table 1). Similarly, expression of Cx26 and Cx31.1 were also unaltered. Transcript of Panx1 but not Panx3 was detected in wild type HeLa cells (Supplementary Figure 2). Stable-transfection of Panx1 resulted in 34 fold rise of its mRNA levels compared to wild type (Table 1). Similarly, over expression of Panx3 resulted in $1.4 \times 10^{-1} \pm 1.8 \times 10^{-2}$ mRNA levels in Panx3-HeLa stable cells (normalized to internal control β-Actin, by $2^{-\Delta C_T}$ method). The real time PCR data along with voltage independent $G_{j(ss)}$ confirm the expression of functional Panx-GJs.

Panx-GJs are permeable to anionic but not cationic dyes. We tested the permeability of different cationic and anionic fluorescent dyes through Panx1-GJs and Panx3-GJs. The dye was injected in one cell (donor cell/cell-1), of a pair through patch pipette and the appearance of fluorescence was followed in the recipient cell (cell-2). Anionic dye Alexa fluor-350 readily diffused through Panx1-GJs and Panx3-GJs as indicated by the increase of fluorescence in the recipient cell within 2–5 minutes of injection (Figure 3A, 3B). However none of the cationic dyes tested e.g. propidium iodide (PI), ethidium bromide (EtBr) and 4′,6-diamidino-2-phenylindole dihydrochloride (DAPI) passed either through Panx1-GJ or Panx3-GJ (Figure 3A, 3B), though the cell pair was strongly coupled, as evident from junctional currents recorded at the end of the experiment. Recipient cell did not show any fluorescence even after 10–15 minutes of dye injection. To confirm that impermeability of cationic

Table 1 | Real time quantification of connexin and pannexin m-RNA levels

Connexin/Pannexin	Relative amount of target mRNA ($2^{-\Delta C_T}$)			Fold change of target mRNA compared to HeLa-(WT), ($2^{-\Delta\Delta G}$)	
	HeLa (WT)	HeLa-Panx1	HeLa-Panx3	HeLa-Panx1	HeLa-Panx3
Cx26	$2.5 \times 10^{-3} \pm 4.1 \times 10^{-4}$	$3.1 \times 10^{-3} \pm 6.0 \times 10^{-4}$ (p = 0.427)	$3.2 \times 10^{-3} \pm 4.1 \times 10^{-4}$ (p = 0.258)	+1.2 fold	+1.3 fold
Cx30	--	--	--	--	--
Cx31.1	$7.0 \times 10^{-4} \pm 1.0 \times 10^{-4}$	$9.8 \times 10^{-4} \pm 1.5 \times 10^{-4}$ (p = 0.075)	$9.2 \times 10^{-4} \pm 2.0 \times 10^{-4}$ (p = 0.180)	+1.6 fold	+1.5 fold
Cx37	--	--	--	--	--
Cx40	--	--	--	--	--
Cx43	--	--	--	--	--
Cx45	$8.3 \times 10^{-3} \pm 2.1 \times 10^{-3}$	$1.0 \times 10^{-2} \pm 1.5 \times 10^{-3}$ (p = 0.407)	$1.0 \times 10^{-2} \pm 2.6 \times 10^{-3}$ (p = 0.548)	+1.4 fold	+1.2 fold
Cx46	--	--	--	--	--
Cx50	--	--	--	--	--
hPanx1	$2.5 \times 10^{-3} \pm 3.0 \times 10^{-4}$	$3.1 \times 10^{-3} \pm 6.0 \times 10^{-4}$ (p = 0.354)	$2.7 \times 10^{-3} \pm 1.9 \times 10^{-4}$ (P = 0.470)	+1.2 fold	+1.1 fold
hPanx3	--	--	--	--	--
rPanx1	--	$9.5 \times 10^{-2} \pm 9.0 \times 10^{-3}$	--	+34 fold**	--
rPanx3	--	--	$1.4 \times 10^{-1} \pm 1.8 \times 10^{-2}$	--	--

h: human; r: rat; $2^{-\Delta CT}$: expression level of target gene normalized to internal control (β-Actin); -- line indicates absence of the target mRNA. Data are averaged from 5 independent experiments.
**P < 0.01. None of the Cxs mRNA showed statistically significant change after Panx expression.

dyes was not due to their sequestration in nucleus, we tested the passage of all these dyes through Cx43-GJ in similar experimental conditions. As shown in figure 3C, Cx43 is permeable to both cationic and anionic dyes. These results suggest the permeability of Panx-GJs favours anions over cations.

Panx-GJs are insensitive to hemichannel blockers and Cx-GJ blockers. We studied the effect of hemichannel blockers and Cx-GJ blockers on Panx-GJs. Surprisingly, Panx1-hemichannel blockers carbenoxolone (CBX) and probenecid had no effect on Panx1-GJs and Panx3-GJs (Figure 4A and 4B). Although 30 μM CBX and 2 mM probenecid blocked Panx1 hemichannels in transfected CHO cells completely (Figure 5B), both Panx1-GJs and Panx3-GJs were unaffected. Even higher concentration of CBX (100 μM) did not alter Panx1-GJ currents. We also looked at the effect of CBX and probenecid on Cx43-GJs. CBX (30 μM) and probenecid (2 mM) inhibited G_j of Cx43-GJs by 30 ± 5% (n = 7) and 42 ± 4% (n = 6) within 5 minutes (Figure 4B). Furthermore, both Panx1-GJs and Panx3-GJs were insensitive to 2 mM heptanol (a commonly used inhibitor of Cx hemichannels and GJs), whereas Cx43-GJs uncoupled completely within 1–2 minutes of heptanol application (Figure 4B). This further implies that junctional channels observed after stable expression of Panxs are not from endogenous Cx-GJs.

We hypothesized that extracellular loops of Panxs constitute the binding sites for CBX and probenecid, as both the blockers are effective from extracellular side. Docking of two hemichannels might restrict the accessibility to the blockers in Panx-GJs. To verify this, we replaced E1 or E2 of Panx1 with the corresponding E1 or E2 of Cx43. As shown in figure 5B, both CBX and probenecid effectively blocked Panx1 hemichannel currents within 1–2 minutes, in transfected CHO cells and in stably transfected Panx1-HeLa cells (Supplementary Figure 3). CBX and probenecid significantly ($p < 0.001$) reduced the current density of Panx1 transfected CHO cells to 6.1 ± 0.7 and 6.5 ± 0.9 pA/pF respectively from control 60 ± 5 pA/pF, measured at +100 mV (table 2). Unlike Cx-GJs, Panx1 hemichannels were insensitive to heptanol (Table 2). Interestingly, Panx3 did not form functional hemichannels in CHO cells (Table 2) and HeLa cells (data not shown), though its expression at the membrane surface was observed in both the cells studied (Supplementary Figures 1 and 4B). Chimeric Panx1, containing E1 of Cx43 (Panx1-E1-Cx43) formed functional hemichannels that exhibited current versus voltage (I-V) plot indistinguishable from the I-V of wild type Panx1 (Figure 5C). The current density of the cells expressing Panx1-E1-Cx43 was comparable to Panx1 expressing cells (Table 2). In agreement with our hypothesis, Panx1-E1-Cx43 hemichannels were insensitive to both CBX and probenecid as shown in the I-V plot generated before and after drug applications (Figure 5C). When the E2 domain of Panx1 (bearing the glycosylation site) was replaced with E2 of Cx43, the surface expression of the chimera was greatly reduced (Supplementary Figure 4A), and also we could not detect any hemichannel activity (Figure 5D).

We could not access the role of extracellular loops of Panx3 in CBX and probenecid mediated inhibition, as Panx3 did not form functional hemichannels. Also the chimeras, Panx3-E1-Cx43 and Panx3-E2-Cx43 did not show any hemichannel activity (Table 2) and their surface expression was greatly reduced compared to WT-Panx3 (Supplementary Figure 4B).

Acidosis and ischemia inhibit pannexin junctions less than connexin junctions. Acidosis created by applying 100% CO_2 has been demonstrated to uncouple many Cx-GJs and at least few innexin GJs[29–31]. Ischemia has been reported to uncouple Cx-GJs, resulting in increased tissue resistance[31–33]. We compared the sensitivity of Panx-GJs to acidosis and ischemia, with that of Cx43-GJ. As shown in figure 6, 5 minutes of CO_2 application reduced the G_j of Panx1-GJ and Panx3-GJ by 37 ± 5% (n = 11) and 27 ± 3% (n = 10)

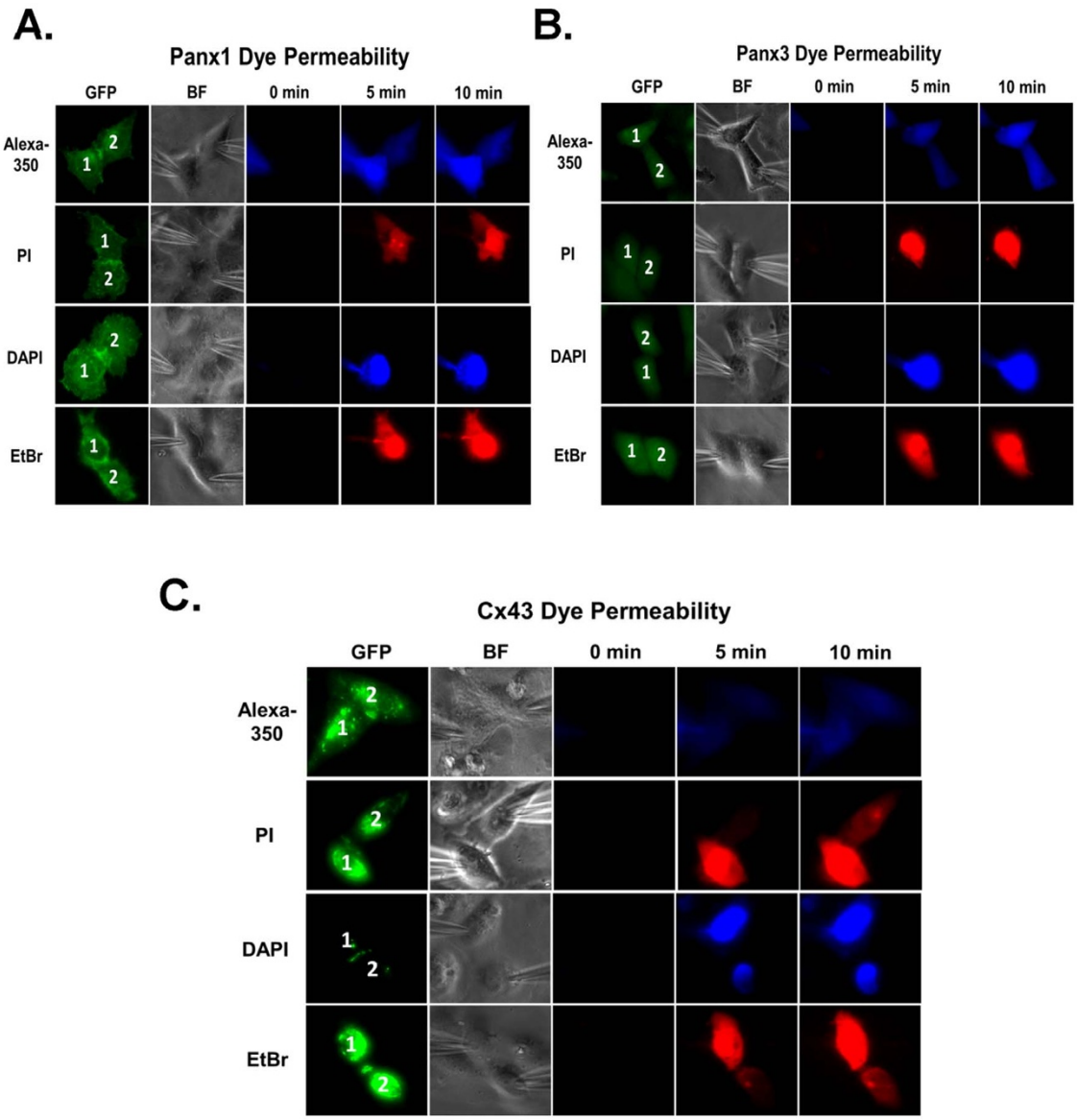

Figure 3 | Pannexin gap junctions are permeable to anionic but not to cationic dyes. Passage of fluorescent dyes through (A) Panx1 and (B) Panx3 GJs. Dye was injected in one cell of a pair (donor cell; Cell-1) through the patch pipette and its passage to the recipient cell (Cell-2) was monitored. In 5 minutes time, anionic Alxa 350 reached to the recipient cell both through Panx1 and Panx3 GJs. None of the cationic dyes (e.g. PI, EtBr and DAPI) passed through Panx1 and Panx3 GJs, indicating the cells are not connected by cytoplasmic bridges. Dyes were not detected in the recipient cells even after 10 minutes. Cell-cell coupling was confirmed in every cell pair by measuring G_j at the end of the experiment. (C) As a positive control, Cx43-GJs expressed in HeLa cells showed the permeation of both anionic and cationic dyes. 'BF' represents bright field image.

respectively. On the other hand, Cx43-GJ uncoupled completely (100%, n = 7) within 1–2 minutes of CO_2 application, in concurrence with earlier studies[29,30]. Ischemia was simulated by depriving oxygen and glucose (oxygen and glucose deprivation: OGD)[32], 5 minutes of OGD uncoupled Panx1-GJ by 33 ± 5% (n = 9) whereas, G_j of Panx3-GJ decreased only by 11 ± 2% (n = 7). In contrast, Cx43-GJ showed much higher sensitivity to OGD. Cx43 showed 52 ± 7% (n = 5) reduction of G_j (Figure 6).

Discussion

The data presented here clearly demonstrate that Panx1 and Panx3 form functional GJs in HeLa cells. Unlike most Cx-GJs, Panx-GJs are insensitive to junctional voltages. Their pharmacological properties are also quite different from known Cx-GJs and Panx hemichannels. Both Panx1 and Panx3 GJs are insensitive to Panx hemichannel blockers CBX and probenecid. Heptanol, though known to uncouple most of the Cx-GJs, has no effect on Panx-GJs.

The ability of Panxs to form functional gap junctions was first shown in *Xenopus* oocyte[3]. Subsequent studies by other groups claimed the same, by demonstrating functional Panx1-GJs and Panx3-GJs when over-expressed in cell lines[8,9]. However several groups could not reproduce the earlier findings in different cell lines and argued that the reported GJs could have resulted from up-regulated endogenous connexins[6,22,23]. Here we document that Panx1 and Panx3, do form functional GJs but in a cell specific manner. Unlike HeLa cells, Panx1 and Panx3 do not form functional GJs in PC-12 cells and N2a cells, though Panx1 readily formed hemichannels in all these cell lines. As shown in the western blot (Figure 2), most Panx1 in PC-12 and N2a cells is glycosylated. Conversely, in HeLa cells only 8% of total Panx1 is glycosylated. Presumably, glycosylation at the extracellular loop of Panx1 hindered the correct docking of hemichannels to form functional GJs in N2a and PC-12 cells. On this basis, it can be expected Panxs can form functional GJs in any cell type, if glycosylation sites are mutated. Unfortunately, removing the

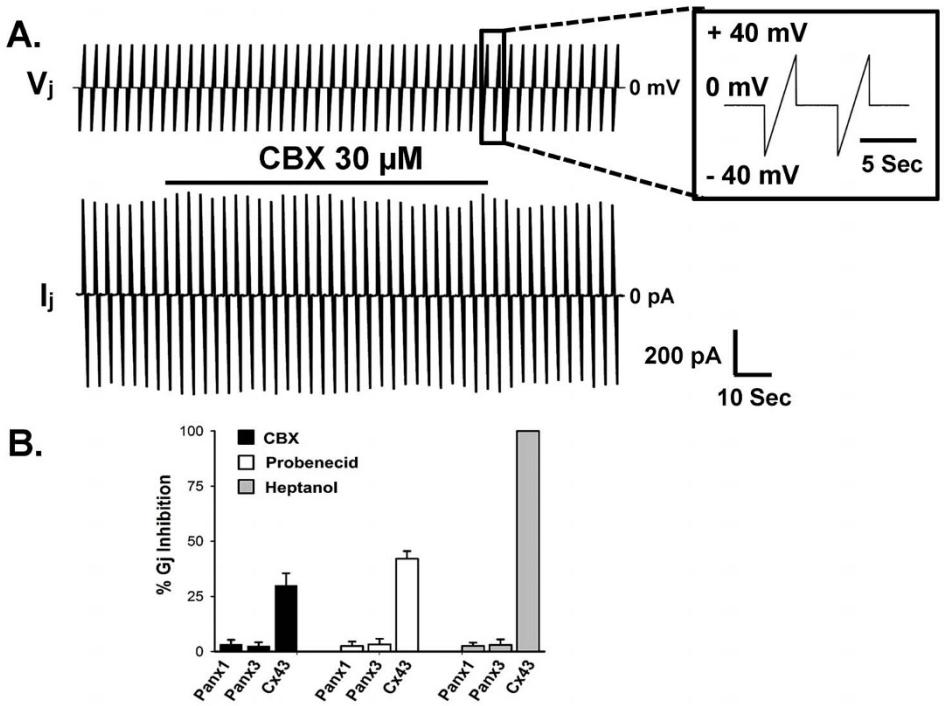

Figure 4 | Pannexin gap junctions are insensitive to CBX, probenecid and heptanol. (A) Representative V_j protocol- and I_j recorded from a Panx1 stably transfected cell pair. I_j was not inhibited in presence of 30 µM CBX. Solid bar over the current trace represents duration of CBX application. (B) Effect of different blockers on G_j of Panx and Cx43 junctions. G_j was measured at +40 mV of V_j. CBX and probenecid (2 mM) did not change the G_j of Panx-GJs in 5 minutes. G_j of Cx43 was reduced by 30–42% with CBX and probenecid, respectively. 2 mM heptanol completely uncoupled Cx43 junctions within 1–2 minutes. However heptanol had no effect on Panx-GJs. Data are the mean ± SEM of 6-11 independent experiments.

glycosylation site (N254 in Panx1 and N71 in Panx3) hinders proper trafficking of Panxs to the plasma membrane surface[6,24] making this study difficult.

mRNAs of Cx26, Cx45 and Cx31.1 were detected in non-transfected wild type HeLa cells, Weak coupling observed in wild type HeLa cells, possibly resulted from Cx45 as evident from the $G_{j(ss)}$-V_j plot: a sharp decrease of $G_{j(ss)}$ with increasing V_j[28]. GJs in HeLa cells resulted from the expression of Panx1 and Panx3, - are not Cx-GJs due to following reasons. i) Expression of Panx1 and Panx3 caused a statistically insignificant 1.2 to 1.6 fold rise in mRNA levels of endogenous Cxs, which cannot account for about the 20 fold rise of junctional currents. ii) Unlike Cx45-GJ (and most other Cx-GJs), $G_{j(ss)}$ of Panx1 and Panx3 expressed cells were independent of V_j. iii) Heptanol and octanol are known to uncouple most Cx-GJs including Cx45- and Cx26-GJs[34]. Whereas GJs formed from the expression of Panx1 and Panx3 were not uncoupled by heptanol. iv) Both Cx45- and Cx26-GJs are permeable to cationic dyes e.g. EtBr, PI and DAPI[26,35]. However, the observed Panx1-GJs and Panx3-GJs were impermeable to these cationic dyes.

In contrast to Panx1 hemichannels, both Panx1- and Panx3-GJs showed insensitivity towards CBX and probenecid (Figure 4). To investigate the reason behind it, we generated chimeric Panx1 having E1 and E2 of Cx43, as Cx43 showed less sensitivity to these drugs. Panx1-E2-Cx43 did not form functional hemichannels, possibly due to removal of the glycosylation site, required for its surface expression[6,24]. Panx1-E1-Cx43 hemichannels showed I-V relations similar to wild type channels, but were not inhibited by CBX or probenecid (Figure 5). The E1 domain of Panx1 is possibly the binding site or part of the binding pocket for CBX and probenecid. However involvement of the E2 domain cannot be ruled out. In Panx1-GJs, docking of E1 and E2 of two hemichannels of neighbouring cells presumably restricted the access of CBX and probenecid. This may also be true for Panx3, as it shares about 62% sequence homology with Panx1[2] and both Panx1 and Panx3 GJs are resistant to CBX and probenecid.

Further, Panx hemichannels have been implicated in ischemic cell death[12,36]. Here, we show that during simulated ischemia (OGD), Panx1-GJs uncoupled moderately, while Panx3-GJs is quite resistant. Therefore, Panx3-GJs may promote survival of ischemic cells by allowing influx of nutrients and metabolites from neighbouring healthy cells.

In conclusion, our data suggest that differential glycosylation underlies cell specific formation of Panx1-GJs. Many proteins have been reported to be differentially glycosylated in several tissues[37,38]. Conceivably, Panxs form GJs in the tissues where they are hypoglycosylated, particularly at their extracellular loops. One major hurdle in the field of GJ research is the lack of specific blockers and most tissues express multiple types of GJs with similar as well as varying properties. The above findings elucidate the distinct properties of Panx-GJs such as insensitivity to heptanol, CBX, probenecid and V_j, which can be exploited to dissect Panx-GJs from Cx-GJs in tissue systems.

Methods

Molecular cloning. c-DNA of rat Panx1-eGFP[39], was kindly provided by Prof. Roberto Bruzzone, HKU-Pasteur Research Centre, Hong Kong. Rat Panx3 c-DNA[3] was provided by Prof. Christian Naus, Department of Cellular and Physiological Sciences, Canada. Mouse Cx43-eGFP, c-DNA was a gift from Prof. Feliksas F. Bukauskas, Albert Einstein College of Medicine, New York[29,30,40]. Panx3 was subcloned into pIRES2-eGFP vector (Clontech, USA) to construct Panx3-IRES2-eGFP. All the plasmids used in this study had CMV promoter. Experiments were performed with eGFP tagged rat Panx1 and rat Panx3-IRES2-eGFP (eGFP and Panx3 are expressed as separate proteins). In eGFP tagged Panx1 and Cx43, eGFP was attached at the carboxyl terminus.

E1 and E2 of Panx1 and Panx3 were replaced with E1 and E2 of Cx43, using two steps PCR based site directed mutagenesis[41]. The resulting chimeras were named as Panx1-E1-Cx43, Panx1-E2-Cx43, Panx3-E1-Cx43 and Panx3-E2-Cx43.

Cell culture. All the cell lines except PC-12 were obtained from National Centre for Cell Science, India. PC-12 cells were procured from Sigma Aldrich, USA. Dulbecco's Modified Eagle's Medium (DMEM), supplemented with 10% heat inactivated foetal bovine serum (FBS), 100 units/ml antimycotic and antibiotic mixture (Gibco, USA) was used to culture N2a, HeLa and CHO cells. PC-12 cells were grown in RPMI

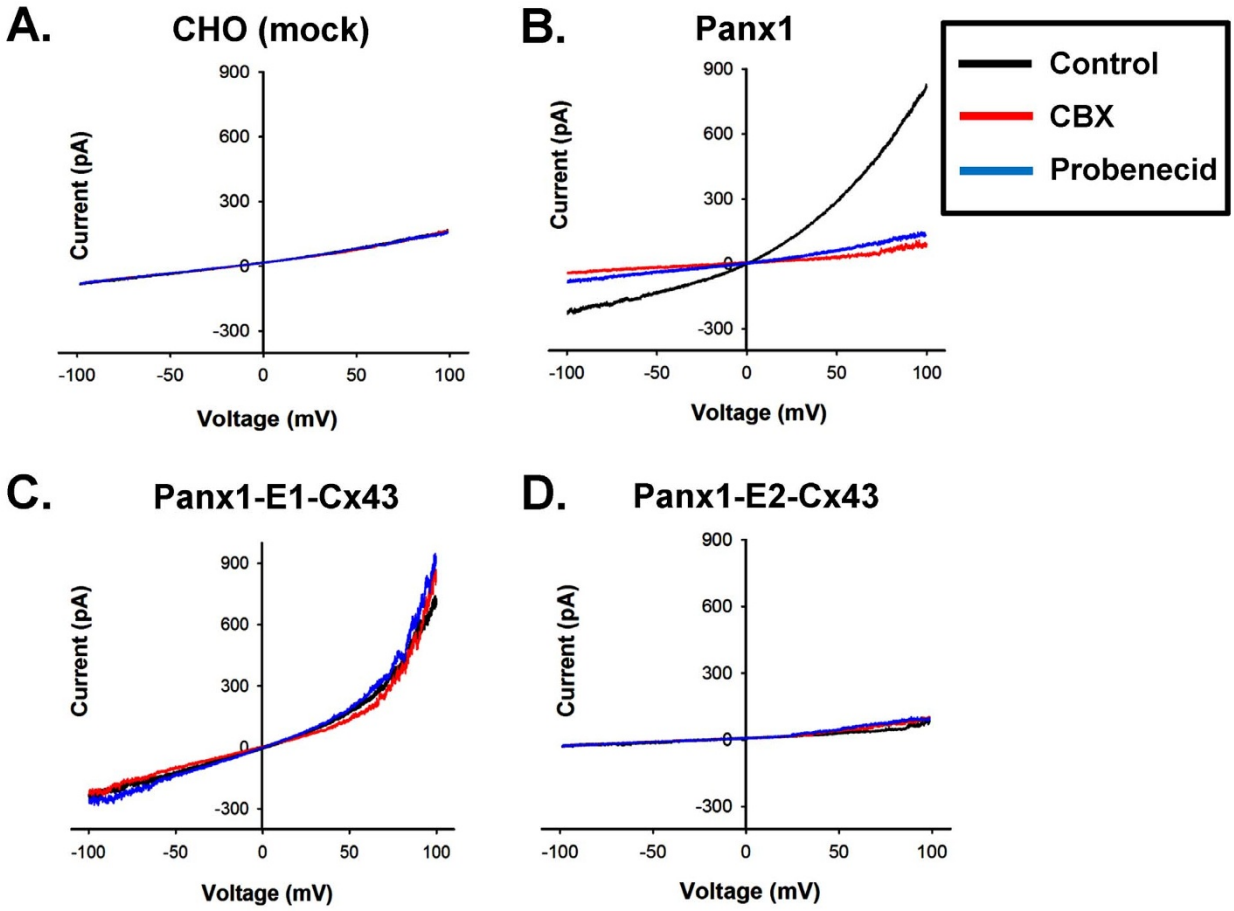

Figure 5 | CBX and probenecid have no effect on chimeric Panx1 hemichannels, bearing the first extracellular loop (E1) of Cx43. (A) I-V curve generated from mock (peGFPN1) transfected CHO cells, did not show Panx1 type currents. (B) I-V curve of Panx1, recorded from transfected CHO cells. Panx1 hemichannel currents were inhibited promptly (within 1–2 min) by 30 μM CBX (red line) and 2 mM probenecid (blue line). (C) Panx1-E1-Cx43 exhibited similar I-V characteristics as wild type Panx1, but was not inhibited either by CBX or by probenecid. (D) I-V curve generated from Panx1-E2-Cx43 did not show significant currents.

medium, supplemented with 10% heat inactivated horse serum, 5% FBS and 100 units/ml antimycotic and antibiotic mixtures (Gibco).

Transfection and generation of stable cell line. Cells were transfected with plasmid DNA using lipofectamine 2000 (Invitrogen, USA). On the day of transfection, growth medium from cells were replaced with medium devoid of FBS and antibiotics. 2 μg of DNA was mixed with 5–6 μl of lipofectamine and incubated for 30 minutes. The DNA-lipofctamine mixture was added to the cells drop wise. After 5 hours, the medium was replaced with normal growth medium and experiments were performed after 24–36 hours of transfection.

For generating stable cell line, first of all, HeLa cells were treated with varying concentrations of G418, ranging from 100 to 1500 μg/ml, for a period of 7–10 days. The minimum concentration of G418 that killed all the cells in 7–10 days was used for selecting the stable clones. In our experimental conditions 750 μg/ml of G418 was found to be effective. After transfecting the cells with Panx1-eGFP or Panx3-IRES2-eGFP (both bearing G418 resistance marker gene), the transfected cells were seeded to the culture media containing 750 μg/ml of G418. Cells were maintained in selection media for 30–45 days with intermittent change to fresh media containing G418. Afterwards, the eGFP expressing single colonies were visualized by fluorescence microscopy and picked by trypsinization with the help of cloning cylinders (Sigma Aldrich, USA) and maintained in selection media. Stable expression was confirmed by real time PCR and/or western blot. All the experiments are performed using cells derived from a single colony.

RNA extraction and quantitative PCR. Total RNA from confluent monolayers of cells were isolated with Trizol reagent (Invitrogen, USA). After DNAse treatment, 5 μg of mRNA was converted to cDNA using oligo-dT primers with the help of an M-MulV Taq, RT-PCR kit (New England Biolabs, USA). Real time PCR based quantification of target mRNA was done using gene specific primers (Supplementary Table 1), with SensiMix SYBR Low-ROX kit (Bioline, USA). Relative levels of mRNA expression are represented in the $2^{-\Delta C_T}$ method[42]. β-actin was used as control for normalization of the C_T (Threshold cycle) values. For determining the fold change in

Table 2 | Average hemichannel current density of pannexins in CHO cells

	Current density (pA/pF)			
Cells	Control (n)	CBX (n)	Probenecid (n)	Heptanol (n)
CHO (mock)	5.25 ± 0.8 (15)	5.3 ± 0.8 (8)	5.6 ± 0.9 (7)	5.3 ± 0.6 (8)
Panx1	60.5 ± 4.6 (23)	6.1 ± 0.7 (15)	6.5 ± 0.9 (12)	68.4 ± 8.1 (7)
Panx1-E1-Cx43	49.2 ± 2.8 (21)	49.1 ± 2.1 (11)	51.6 ± 2.6 (10)	52.3 ± 3.5 (8)
Panx1-E2-Cx43	6.1 ± 1.0 (11)	6.0 ± 1.0 (7)	6.0 ± 1.1 (5)	6.2 ± 1.4 (5)
Panx3	6.3 ± 0.7 (15)	7.0 ± 0.8 (10)	6.2 ± 0.8 (7)	6.3 ± 1.0 (5)
Panx3-E1-Cx43	5.8 ± 1.2 (5)	5.2 ± 1.5 (4)	5.4 ± 1.1 (3)	5.7 ± 1.3 (3)
Panx3-E2-Cx43	6.1 ± 1.4 (6)	5.9 ± 1.2 (4)	6.0 ± 1.3 (4)	6.2 ± 1.1 (3)

Values are mean ± SEM; n, number of cells studied.

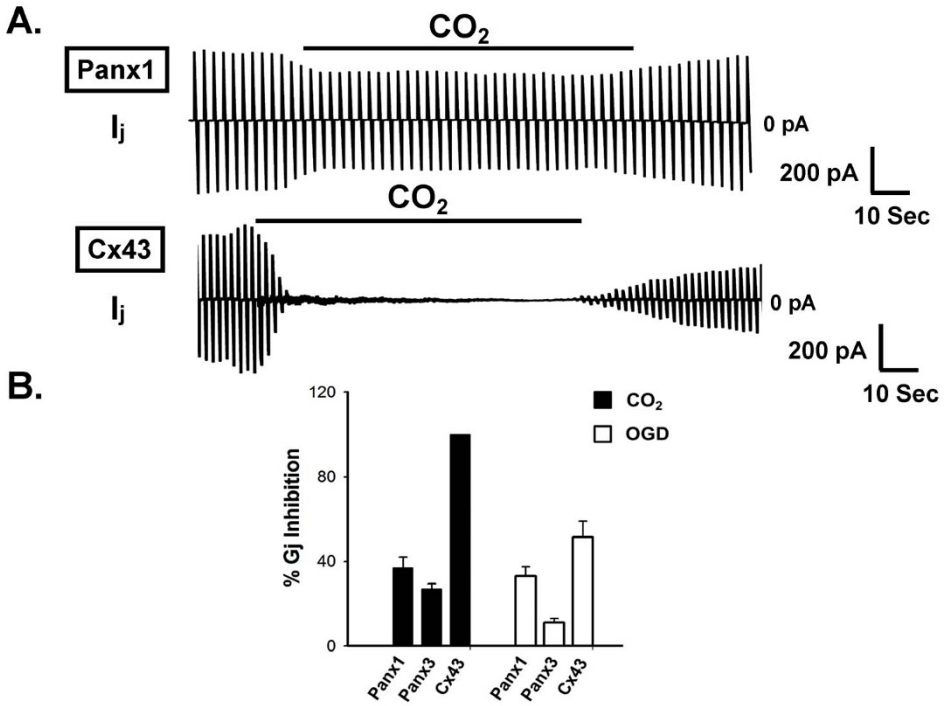

Figure 6 | Acidosis and Oxygen glucose deprivation (OGD) uncoupled Pannnexin junctions to a lesser extent than Cx43 junction. Acidosis was achieved by saturating external solution with 100% CO_2. (A) Representative junctional current traces showing the effect of CO_2 on Panx1-GJs and Cx43-GJs. Although CO_2 uncoupled Cx43 junction rapidly it had little inhibitory effect on Panx junctions. Solid lines over the current traces represent duration of CO_2 application. (B) Inhibition of G_j by CO_2 and OGD. OGD was achieved as described in the method section. Both Panx1-GJs and Panx3-GJs were inhibited by CO_2 and OGD to much lesser extent, compared to Cx43-GJs. Values are the mean ± SEM of 7-11 experiments.

expression, the $2^{-\Delta\Delta C_T}$ method of representation was followed[42]. Equal amounts of cDNA were used for all experimental sets.

qPCR inhibition assay. The absence of inhibitors in qPCR was confirmed using Alien RNA transcript (Alien qRT-PCR Inhibitor Alert, Agilent Technologies, CA, USA). The RNA sample was spiked with Alien RNA (5×10^4 copies/µl) before reverse transcription reaction. The C_T values for Alien RNA with water (control) and Alien RNA with sample RNA (test) was compared after real time PCR by subtracting the C_T value of control from C_T value of test.

Western blotting. Cells were harvested using cell scraper, followed by centrifugation at 2500 × g for 2 minutes and then re-suspended in lysis buffer (0.1 mM Tris-HCl (pH 8.0), 2 mM EDTA, 150 mM NaCl and 1% NP40), supplemented with protease inhibitor cocktail (Sigma Aldrich). After incubating at 4°C for 45 minutes the lysed cells were centrifuged at 2500 × g for 10 minutes at 4°C. Supernatant containing 50 µg of protein was subjected to SDS-polyacrylamide gel electrophoresis, using 8% separating gel. After electrophoresis proteins were transferred to polyvinylidene fluoride (PVDF) membrane (Bio-Rad, USA), followed by blocking with 2% bovine serum albumin (BSA) and 0.05% Tween-20 in Tris-buffered saline (TBS) for 1 hour at room temperature (22–24°C). The blot was incubated overnight with mouse monoclonal antibody against eGFP (SC-9996; Santa Cruz Biotechnology, USA) at 1 : 1000 dilution at 4°C. After several washes with TBS-Tween-20 solution, the blot was incubated for 1 hour with HRP conjugated secondary antibody (SC-2371; Santa Crutz Biotechnology) at 1 : 2000 dilution at room temperature. Specific protein bands were visualized on X-ray film (Amersham, USA), after treating the blot with super signal west pico-chemiluminescent substrate (Thermo Scientific, USA). For confirming the glycosylation, cell extracts (50 µg of total protein) were incubated with 10 units of PNGase-F (Sigma Aldrich) for 30 minutes at 37°C before loading them on to a gel.

Immunofluorescence. Cells were fixed with 4% paraformaldehyde for 20 minutes, washed thoroughly with 1X phosphate buffer saline (PBS; Gibco) followed by blocking with 10% FBS and 0.3% triton X-100 in 1X PBS, for 1 hour. After blocking, cells were incubated overnight with goat polyclonal Panx3 antibody (SC-51387; Santa Cruz Biotechnology) at 4°C at 1 : 100 dilution. After wash, the cells were counterstained with anti-goat-594 secondary antibody (A11080; Invitrogen, USA) for one hour at room temperature (22–24°C) at 1 : 500 dilution. Nuclei were stained with 1 µM DAPI (Molecular Probes, USA). A Zeiss laser scanning confocal microscope was used for capturing images.

Patch clamp recording. Channel currents were recorded with an Axopatch 200B patch clamp amplifier (Molecular Devices, USA). Digidata 1440 and pClamp10 (Molecular Devices) were used for digitization and data acquisition/analysis. The bath solution contained (in mM) 150 NaCl, 5 KCl, 1 $MgCl_2$, 5 HEPES (pH 7.4), 10 D-glucose and 2 $CaCl_2$. The pipette solution contained (in mM) 10 NaCl, 140 KCl, 1 $MgCl_2$, 0.2 $CaCl_2$, 3 Mg-ATP, 10 HEPES (pH 7.2) and 2 EGTA unless otherwise mentioned. For measuring junctional currents (I_j), two coupled cells were patched simultaneously with two separate amplifiers. Initially both cells were held at 0 mV. Holding potentials of cell-1 and cell-2 are designated as V_1 and V_2 respectively. To create a transjunctional voltage (V_j) difference ($V_j = V_1 - V_2$), V_1 was stepped to different voltages, keeping V_2 at 0 mV. The current recorded from cell-2, represents the junctional current ($I_j = -I_2$). For pharmacological characterization, −40 mV to +40 mV voltage ramps of 4 second duration were applied to one cell of the pair. 4 second recovery at 0 mV was allowed between successive sweeps. I_j was continuously recorded from the second cell held at 0 mV. For recording hemichannel activity, −100 mV to +100 mV voltage ramps for 5 sec in duration, with 10 sec interval between ramps were used. Current density was calculated by normalizing the hemichannel currents recorded at +100 mV with capacitance of that cell.

Dye permeability studies. For dye permeability studies, different fluorophores were included in the pipette solution at a final concentration of 0.1 mM. Anionic dye Alexa fluor-350 (Alexa-350: charge -1, MW 349; Molecular probes, USA) and cationic dyes: propidium iodide (PI: charge +2, MW 668; Sigma Aldrich, USA), 4′, 6-diamidino-2-phenylindole dihydrochloride (DAPI: charge +2, MW 350; Molecular probes) and ethidium bromide (EtBr: charge +1, MW 394; Sigma Aldrich) were used. Dye was administered in one of the cells of a pair through a patch pipette and allowed to equilibrate. Transfer of the dye to the second cell was monitored by capturing the images at 5, 10 and 15 minutes. Junctional conductance (G_j) was measured at the end of the experiment by making whole cell in the coupled cell with another patch pipette.

Acidosis and ischemia. For creating acidosis, 100% CO_2 was bubbled to the HEPES containing external bath solution. Ischemia was simulated by exposing cells to oxygen and glucose free solution, as described in our and many earlier reports[32,36,43]. Briefly, cells were bathed first with control bicarbonate solution (pH 7.4) containing (in mM) 124 NaCl, 4 KCl, 26 $NaHCO_3$, 1.5 NaH_2PO_4, 1.5 $MgSO_4$, 10 D-glucose and 2 $CaCl_2$. The solution was continuously bubbled with 5% CO_2 and 95% air, at room temperature. OGD was created by replacing the control bath solution with ischemic solution (IS), which had essentially same composition as control, with the exception of 10 mM sucrose instead of D-glucose. IS was degassed (by putting in desiccator) for 1 hour followed by continuous bubbling with mixed gas containing 5% CO_2 and 95% of Argon. To assure complete removal of dissolved O_2, O_2 scavenger sodium dithionite (2 mM) was added.

Statistical analysis. Data provided here are representative of 5–7 independent experiments. Values are mean ± SEM of 5–25 replicates as described in the results section and figure legends. A paired student t-test was performed for comparison between two groups, and a p value < 0.05 was considered as statistical significant.

1. Panchin, Y. *et al.* A ubiquitous family of putative gap junction molecules. *Curr Biol* **10**, R473–474 (2000).
2. Baranova, A. *et al.* The mammalian pannexin family is homologous to the invertebrate innexin gap junction proteins. *Genomics* **83**, 706–716 (2004).
3. Bruzzone, R. *et al.* Pannexins, a family of gap junction proteins expressed in brain. *Proc Natl Acad Sci U S A* **100**, 13644–13649 (2003).
4. Panchin, Y. V. Evolution of gap junction proteins--the pannexin alternative. *J Exp Biol* **208**, 1415–1419 (2005).
5. Swayne, L. A., Sorbara, C. D. & Bennett, S. A. Pannexin 2 is expressed by postnatal hippocampal neural progenitors and modulates neuronal commitment. *J Biol Chem* **285**, 24977–24986 (2010).
6. Penuela, S. *et al.* Pannexin 1 and pannexin 3 are glycoproteins that exhibit many distinct characteristics from the connexin family of gap junction proteins. *J Cell Sci* **120**, 3772–3783 (2007).
7. Wang, X. H., Streeter, M., Liu, Y. P. & Zhao, H. B. Identification and characterization of pannexin expression in the mammalian cochlea. *J Comp Neurol* **512**, 336–346 (2009).
8. Ishikawa, M. *et al.* Pannexin 3 functions as an ER Ca^{2+} channel, hemichannel, and gap junction to promote osteoblast differentiation. *J Cell Biol* **193**, 1257–1274 (2011).
9. Vanden Abeele, F. *et al.* Functional implications of calcium permeability of the channel formed by pannexin 1. *J Cell Biol* **174**, 535–546 (2006).
10. Lai, C. P. *et al.* Tumor-suppressive effects of pannexin 1 in C6 glioma cells. *Cancer Res* **67**, 1545–1554 (2007).
11. Celetti, S. J. *et al.* Implications of pannexin 1 and pannexin 3 for keratinocyte differentiation. *J Cell Sci* **123**, 1363–1372 (2010).
12. Bargiotas, P. *et al.* Pannexins in ischemia-induced neurodegeneration. *Proc Natl Acad Sci U S A* **108**, 20772–20777 (2011).
13. Kim, J. E. & Kang, T. C. The P2X7 receptor-pannexin-1 complex decreases muscarinic acetylcholine receptor-mediated seizure susceptibility in mice. *J Clin Invest* **121**, 2037–2047 (2011).
14. Ma, W., Hui, H., Pelegrin, P. & Surprenant, A. Pharmacological characterization of pannexin-1 currents expressed in mammalian cells. *J Pharmacol Exp Ther* **328**, 409–418 (2009).
15. Silverman, W. R. *et al.* The pannexin 1 channel activates the inflammasome in neurons and astrocytes. *J Biol Chem* **284**, 18143–18151 (2009).
16. Bao, L., Locovei, S. & Dahl, G. Pannexin membrane channels are mechanosensitive conduits for ATP. *FEBS Lett* **572**, 65–68 (2004).
17. Chekeni, F. B. *et al.* Pannexin 1 channels mediate 'find-me' signal release and membrane permeability during apoptosis. *Nature* **467**, 863–867 (2010).
18. Sandilos, J. K. *et al.* Pannexin 1, an ATP release channel, is activated by caspase cleavage of its pore-associated C-terminal autoinhibitory region. *J Biol Chem* **287**, 11303–11311 (2012)
19. Poornima, V. *et al.* P2X7 receptor-pannexin 1 hemichannel association: effect of extracellular calcium on membrane permeabilization. *J Mol Neurosci* **46**, 585–594 (2012).
20. Locovei, S. *et al.* Pannexin1 is part of the pore forming unit of the $P2X_7$ receptor death complex. *FEBS Lett* **581**, 483–488 (2007).
21. Iglesias, R. *et al.* P2X7 receptor-Pannexin1 complex: pharmacology and signaling. *Am J Physiol Cell Physiol* **295**, C752–760 (2008).
22. Huang, Y., Grinspan, J. B., Abrams, C. K. & Scherer, S. S. Pannexin1 is expressed by neurons and glia but does not form functional gap junctions. *Glia* **55**, 46–56 (2007).
23. Sosinsky, G. E. *et al.* Pannexin channels are not gap junction hemichannels. *Channels (Austin)* **5**, 193–7 (2011).
24. Boassa, D. *et al.* Pannexin1 channels contain a glycosylation site that targets the hexamer to the plasma membrane. *J Biol Chem* **282**, 31733–31743 (2007).
25. Cao, F. *et al.* A quantitative analysis of connexin-specific permeability differences of gap junctions expressed in HeLa transfectants and *Xenopus* oocytes. *J Cell Sci* **111**, 31–43 (1998).
26. Elfgang, C. *et al.* Specific permeability and selective formation of gap junction channels in connexin-transfected HeLa cells. *J Cell Biol* **129**, 805–817 (1995).
27. Hennemann, H. *et al.* Two gap junction genes, connexin 31.1 and 30.3, are closely linked on mouse chromosome 4 and preferentially expressed in skin. *J Biol Chem* **267**, 17225–17233 (1992).
28. Elenes, S. *et al.* Heterotypic docking of Cx43 and Cx45 connexons blocks fast voltage gating of Cx43. *Biophys J* **81**, 1406–1418 (2001).
29. Bukauskas, F. F., Bukauskiene, A., Bennett, M. V. & Verselis, V. K. Gating properties of gap junction channels assembled from connexin43 and connexin43 fused with green fluorescent protein. *Biophys J* **81**, 137–152 (2001).
30. Bukauskas, F. F., Angele, A. B., Verselis, V. K. & Bennett, M. V. Coupling asymmetry of heterotypic connexin 45/connexin 43-EGFP gap junctions: properties of fast and slow gating mechanisms. *Proc Natl Acad Sci U S A* **99**, 7113–7118 (2002).
31. Beardslee, M. A. *et al.* Dephosphorylation and intracellular redistribution of ventricular connexin43 during electrical uncoupling induced by ischemia. *Circ Res* **87**, 656–662 (2000).
32. Sahu, G. & Bera, A. K. Contribution of intracellular calcium and pH in ischemic uncoupling of cardiac gap junction channels formed of connexins 43, 40, and 45: a critical function of C-terminal domain. *PLoS One* **8**, e60506 (2013).
33. Smith, W. T. th *et al.* The Ib phase of ventricular arrhythmias in ischemic in situ porcine heart is related to changes in cell-to-cell electrical coupling. Experimental Cardiology Group, University of North Carolina. *Circulation* **92**, 3051–3060 (1995).
34. Skeberdis, V. A. *et al.* pH-dependent modulation of connexin-based gap junctional uncouplers. *J Physiol* **589**, 3495–506 (2011).
35. Rackauskas, M., Verselis, V. K. & Bukauskas, F. F. Permeability of homotypic and heterotypic gap junction channels formed of cardiac connexins mCx30.2, Cx40, Cx43, and Cx45. *Am J Physiol Heart Circ Physiol* **293**, H1729–1736 (2007).
36. Thompson, R. J., Zhou, N. & MacVicar, B. A. Ischemia opens neuronal gap junction hemichannels. *Science* **312**, 924–927 (2006).
37. Somerville, R. A. & Ritchie, L. A. Differential glycosylation of the protein (PrP) forming scrapie-associated fibrils. *J Gen Virol* **71**, 833–839 (1990).
38. Kumagai, A. K., Dwyer, K. J. & Pardridge, W. M. Differential glycosylation of the GLUT1 glucose transporter in brain capillaries and choroid plexus. *Biochim Biophys Acta* **1193**, 24–30 (1994).
39. Bruzzone, R., Barbe, M. T., Jakob, N. J. & Monyer, H. Pharmacological properties of homomeric and heteromeric pannexin hemichannels expressed in *Xenopus* oocytes. *J Neurochem* **92**, 1033–1043 (2005).
40. Bukauskas, F. F., Bukauskiene, A. & Verselis, V. K. Conductance and permeability of the residual state of connexin43 gap junction channels. *J Gen Physiol* **119**, 171–185 (2002).
41. Rubin, J. B., Verselis, V. K., Bennett, M. V. & Bargiello, T. A. A domain substitution procedure and its use to analyze voltage dependence of homotypic gap junctions formed by connexins 26 and 32. *Proc Natl Acad Sci U S A* **89**, 3820–3824 (1992).
42. Schmittgen, T. D. & Livak, K. J. Analyzing real-time PCR data by the comparative C_T method. *Nat Protoc* **3**, 1101–1108 (2008).
43. Diarra, A. *et al.* Anoxia-evoked intracellular pH and Ca^{2+} concentration changes in cultured postnatal rat hippocampal neurons. *Neuroscience* **93**, 1003–1016 (1999).

Acknowledgments

We thank Dr. Anjana Chandrasekhar and S. Divya for critical comments on the manuscript. We sincerely acknowledge R. Suryaraja for his help in confocal microscopy. This work was supported by the Indian Council of Medical Research.

Author contributions

G.S. and A.K.B.: conceived the idea, analysed data and wrote the manuscript. G.S. and S.S.: performed experiments.

Additional information

Supplementary information accompanies this paper at http://www.nature.com/scientificreports

Competing financial interests: The authors declare no competing financial interests.

How to cite this article: Sahu, G., Sukumaran, S. & Bera, A.K. Pannexins form gap junctions with electrophysiological and pharmacological properties distinct from connexins. *Sci. Rep.* **4**, 4955; DOI:10.1038/srep04955 (2014).

This work is licensed under a Creative Commons Attribution-NonCommercial-NoDerivs 3.0 Unported License. The images in this article are included in the article's Creative Commons license, unless indicated otherwise in the image credit; if the image is not included under the Creative Commons license, users will need to obtain permission from the license holder in order to reproduce the image. To view a copy of this license, visit http://creativecommons.org/licenses/by-nc-nd/3.0/